Bulletin of Mathematical Biology (1999) **61**, 1121–1149
Article No. bulm.1999.0136
Available online at http://www.idealibrary.com on IDEAL

Multiple Attractors, Saddles, and Population Dynamics in Periodic Habitats

SHANDELLE M. HENSON*
Department of Mathematics,
University of Arizona,
Tucson, AZ 85721,
U.S.A.
E-mail: henson@math.arizona.edu

R. F. COSTANTINO
Department of Biological Sciences,
University of Rhode Island,
Kingston, RI 02881,
U.S.A.
E-mail: rcos@uri.edu

J. M. CUSHING
Department of Mathematics,
Interdisciplinary Program in Applied Mathematics,
University of Arizona,
Tucson, AZ 85721,
U.S.A.
E-mail: cushing@math.arizona.edu

BRIAN DENNIS
Department of Fish and Wildlife Resources
and Division of Statistics,
University of Idaho,
Moscow, ID 83844,
U.S.A.
E-mail: brian@uidaho.edu

ROBERT A. DESHARNAIS
Department of Biology and Microbiology,
California State University,
Los Angeles, CA 90032,
U.S.A.
E-mail: rdeshar@calstatela.edu

Mathematical models predict that a population which oscillates in the absence of time-dependent factors can develop multiple attracting final states in the advent of

*Author to whom correspondence should be addressed; current address: Department of Mathematics, College of William and Mary, Williamsburg, VA 23187, U.S.A.

0092-8240/99/061121 + 29 $30.00/0

periodic forcing. A periodically-forced, stage-structured mathematical model predicted the transient and asymptotic behaviors of *Tribolium* (flour beetle) populations cultured in periodic habitats of fluctuating flour volume. Predictions included multiple (2-cycle) attractors, resonance and attenuation phenomena, and saddle influences. Stochasticity, combined with the deterministic effects of an unstable 'saddle cycle' separating the two stable cycles, is used to explain the observed transients and final states of the experimental cultures. In experimental regimes containing multiple attractors, the presence of unstable invariant sets, as well as stochasticity and the nature, location, and size of basins of attraction, are all central to the interpretation of data.

1. INTRODUCTION

Successful prediction of a population's response to a fluctuating environment is rare, even in the simplified realm of the laboratory. Indeed, few controlled experimental studies have addressed the effect of time-variant factors, and most mathematical models are autonomous (do not depend explicitly on time).

An exception is the laboratory experiment conducted by Jillson (1980) and the subsequent model-based explanation proposed by Costantino *et al*. (1998). For a different interpretation of the Jillson experiment see Nisbet and Gurney (1981) and Renshaw (1991). Jillson placed beetles in volumes of flour that alternated between 32 g and 8 g every two weeks. The control cultures remained in a constant volume of 20 g. Jillson found that total population numbers in the periodically-fluctuating environment were more than twice those in the constant environment, even though the average flour volume was the same in both cases.

To explain this phenomenon, the discrete LPA *Tribolium* model of Dennis *et al*. (1995, 1997) and Costantino *et al*. (1995, 1997) was modified by Henson and Cushing (1997) and Costantino *et al*. (1998) to account for the periodic flour volume. Cannibalism between life cycle stages is the nonlinear mechanism driving flour beetle dynamics in these experiments (Park *et al*., 1970). Habitat size was incorporated into the model by the hypothesis that all rates of cannibalism are inversely proportional to the volume of the culture medium. The 'periodic LPA model' correctly described the larger total population size in the 32–8 g periodic habitat. It also correctly described the phase relationships and transient dynamics observed in the Jillson data. The periodic LPA model explained the increased average biomass observed in the 32–8 g habitat as a type of resonance in which the inherent biological oscillation resonates with the periodic habitat (Costantino *et al*., 1998). In this sense, we are referring to 'resonance' as an increase in the *average* of an output oscillation in response to a tuning of the *amplitude* of the input oscillation.

In fact, discrete mathematical models predict fairly general resonance and multiple attractor phenomena in the presence of periodic forcing. Henson (1999) shows that populations which cycle in the absence of time-dependent factors can develop multiple attracting oscillatory final states in the advent of periodic forcing. Some of the multiple final states may resonate with the periodic forcing in the above sense, while others may attenuate, depending on the phase difference between the input and output oscillations. The prospect of multiple stable states has long been known to be a prediction of various nonlinear population models (May, 1977), but to date few convincing examples of multiple stable states have been documented (Petraitis and Latham, 1999).

In a specific application of this general theoretical forecast, we used the periodic LPA model to generate new predictions testable in the laboratory, and then carried out the indicated experiments. When the relative amplitude of oscillating flour volume in the periodic LPA model was set at 40% to simulate a 28–12 g alternating habitat, the model predicted multiple attracting final states: two different 2-cycles out-of-phase with each other and differing in average magnitude of animal numbers. We tested this model forecast in the laboratory by placing and maintaining beetle cultures in the different (model predicted) basins of attraction of the two locally stable 2-cycles.

We were able to identify the effects of the multiple attractors in beetle population numbers. Furthermore, natural stochasticity combined with the effects of an unstable 'saddle cycle' separating the two stable cycles greatly influenced the transients and final states of the experimental populations, making the unstable saddle central to the interpretation of the data.

Section 2 illustrates, by means of a simple univariate Ricker-type map, the general phenomenon of multiple attractors predicted by periodically-forced models. In Section 3, we introduce the multivariate periodically-forced LPA model for stage-structured *Tribolium* dynamics as a specific application of the theory. In Section 4 we analyse the model's predictions of multiple attractors and saddles and outline the design of experiments. Section 5 describes the protocol for two experiments constructed to test the model's predictions. Sections 6 and 7 present the results of the experiments. In Section 8, we briefly discuss some features of the modeling methodology and summarize the project.

2. MULTIPLE ATTRACTORS AND PERIODICALLY-FORCED MODELS

We first illustrate the general mathematical theory of multiple attractors in periodically-forced models by means of a discrete univariate Ricker-type map

$$x_{t+1} = f_0(x_t) = bx_t e^{-cx_t} + (1-\mu)x_t$$

which predicts the density of individuals x_{t+1} in a population at census $t+1$ given the density of individuals x_t at census t. Here $b > 0$ is the inherent per capita

recruitment rate per census interval at small population sizes, and e^{-cx_t} represents the fractional reduction of recruitment due to density-dependent effects. Also, $0 \leq \mu \leq 1$ is the fraction of individuals expected to die during one census period. When $\mu = 1$, the map becomes the well-known Ricker model.

This model is autonomous, and predicts 2-cycles at many values of its parameters. For example, if $b = 40$, $c = 1$, and $\mu = 0.93$, the sequence $x_0 = 1.035$, $x_1 = 14.78$, $x_2 = 1.035$, $x_3 = 14.78, \ldots$ is a 2-cycle solution (to 4 significant figures). Initial conditions near $x_0 = 1.035$ lead to solutions approaching this 2-cycle; hence, the 2-cycle is 'locally stable'. The phase-shifted cycle $x_0 = 14.78$, $x_1 = 1.035$, $x_2 = 14.78$, $x_3 = 1.035, \ldots$ is also a locally stable 2-cycle solution. The set of values $\{1.035, 14.78\}$ is an 'attractor' for the map. Both 2-cycles 'live' on this attractor. The set of initial conditions x_0 which generate solutions converging to either of the 2-cycles is the 'basin of attraction' for the attractor.

Suppose periodic-forcing is introduced, for example into recruitment, so that the birth rate oscillates with relative amplitude $0 < \alpha < 1$ and average b:

$$x_{t+1} = f_\alpha(t, x_t) = b[1 + \alpha(-1)^t]x_t e^{-cx_t} + (1 - \mu)x_t.$$

If the relative amplitude α is increased slightly from zero, for example to $\alpha = 0.01$, the first 2-cycle listed above is no longer a solution, but is 'perturbed' into a locally stable 2-cycle solution $x_0 = 1.045$, $x_1 = 14.92$, $x_2 = 1.045$, $x_3 = 14.92, \ldots$ of the periodically-forced model. This 2-cycle has the same phase as its parent cycle, but has a larger average (is 'resonant'). Similarly, the second 2-cycle solution of the autonomous model is perturbed into a locally stable 2-cycle solution $x_0 = 14.64$, $x_1 = 1.025$, $x_2 = 14.64$, $x_3 = 1.025, \ldots$ of the periodically-forced model. This perturbed cycle also preserves the phase of the parent cycle, but has smaller average (is 'attenuant'). It is easy to check that the phase shifts of the 2-cycle solutions of the periodically-forced model are not themselves solutions.

In terms of attractors, the single attractor $\{1.035, 14.78\}$ of the autonomous model has been perturbed into two different attractors $\{1.045, 14.92\}$ and $\{1.025, 14.64\}$ of the periodically-forced model. Although the attractor of the autonomous model is associated with two solutions of different phases, the attractors of the periodically-forced model are associated with unique solutions of opposite phases.

In general, if an autonomous discrete model having a stable p-cycle solution is subjected to small amplitude p-periodic forcing, the p-cycle attractor will split into p p-cycle attractors associated with p different phases (Henson, 1999). That is, mathematical models predict that a population which oscillates with minimal period p in the absence of periodic forcing will develop p out-of-phase attracting oscillatory final states in the advent of small amplitude forcing of minimal period p. Although the theory only guarantees multiple attractors for 'small' amplitude forcing, they often persist at larger amplitudes as well.

We close this section with two further remarks. First, the Ricker-type model illustrates another typical, though somewhat less general, phenomenon connected

to the one discussed above. The autonomous model has a unique equilibrium $x = c^{-1}ln(b/\mu) \approx 3.762$ (that is, a constant solution sequence $x_0 = 3.762$, $x_1 = 3.762$, $x_2 = 3.762, \ldots$) which can be found by solving the fixed point equation $x = bxe^{-cx} + (1 - \mu)x$. The equilibrium is unstable at the given parameter values of b, c, and μ. The periodically-forced model does not admit an equilibrium solution. However, when the relative amplitude is perturbed from $\alpha = 0$ to $\alpha = 0.01$, the unstable equilibrium $x = 3.762$ of the autonomous model is perturbed into an unstable 2-cycle solution $x_0 = 3.785$, $x_1 = 3.738$, $x_2 = 3.785$, $x_3 = 3.738, \ldots$ of the periodically-forced model. Figure 1(a) illustrates the values of all three perturbed cycles as functions of the amplitude parameter α. As α increases, the unstable cycle and the attenuant stable cycle of the same phase annihilate each other in a 'saddle-node bifurcation', while the resonant stable cycle persists for all $\alpha < 1$. The existence of such an unstable cycle and saddle-node bifurcation will be important to our specific multivariate application.

Second, all the above 2-cycles can be studied as fixed points of the composite map $x_{t+1} = f_\alpha(1, f_\alpha(0, x_t))$. Given an initial condition, the orbit generated by the composite map corresponds to every other step of the orbit generated by the map $x_{t+1} = f_\alpha(t, x_t)$ (see Henson *et al*., 1998). Thus, in the context of the composite map, $x = 1.035$ and $x = 14.78$ are both locally stable fixed points when $\alpha = 0$, while $x = 3.762$ is an unstable fixed point. If α is increased from zero to $\alpha = 0.01$ in the composite map, the first stable fixed point is perturbed into a new stable fixed point $x = 1.045$, the second stable fixed point is perturbed into a stable fixed point $x = 14.64$, and the unstable fixed point is perturbed into an unstable fixed point $x = 3.785$. In terms of attractors, the two attractors {1.035} and {14.78} of the composite map with $\alpha = 0$ are perturbed into the two attractors {1.045} and {14.64} of the composite map when α is increased to $\alpha = 0.01$. In our specific multivariate application, the composite model will be helpful in presenting and evaluating model predictions.

In the next two sections we apply this general theory of multiple attractors and periodicity to a specific validated multivariate population model (the LPA model), and generate the predictions tested in the laboratory.

3. THE MODEL

The autonomous LPA model is given by the equations

$$\begin{aligned} L_{t+1} &= bA_t \exp(-c_{ea}A_t - c_{el}L_t) \\ P_{t+1} &= (1 - \mu_l)L_t \\ A_{t+1} &= P_t \exp(-c_{pa}A_t) + (1 - \mu_a)A_t \end{aligned} \tag{1}$$

where L_t denotes the number of (feeding) larvae, P_t denotes the number of pupae (nonfeeding larvae, pupae, and callow adults), and A_t denotes the number of

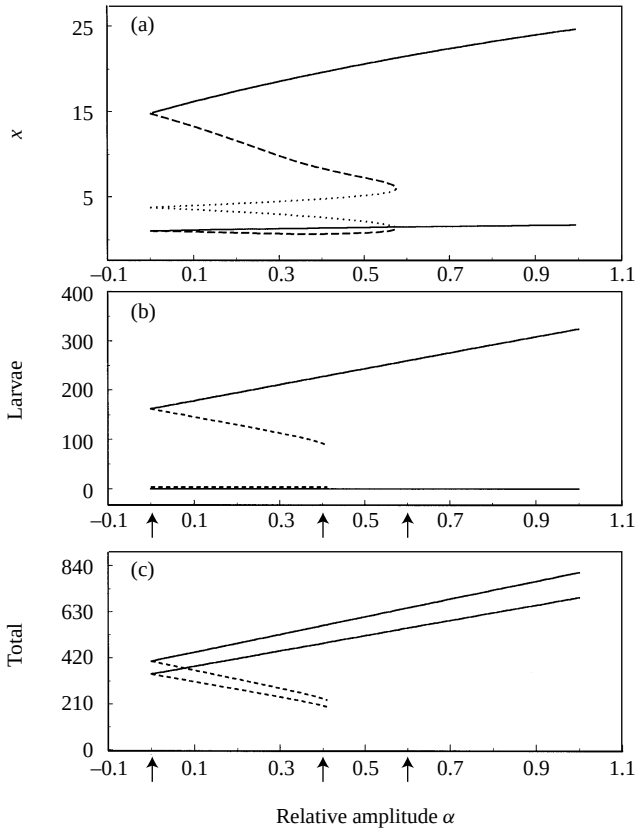

Figure 1. Model predictions. (a) 2-cycle solutions of the periodically-forced Ricker-type map, shown as functions of amplitude α. When $\alpha = 0$, there are two stable 2-cycles which are simply time shifts of each other, and an unstable fixed point. As α increases from zero, one of the two locally stable 2-cycles increases in average (solid lines), while the other decreases in average (dashed lines). The unstable fixed point is perturbed into an unstable 2-cycle (dotted lines). The attenuant stable cycle and the unstable cycle annihilate each other in a saddle-node bifurcation, while the resonant stable cycle persists for all $\alpha < 1$. (b) Larval component of 2-cycle solutions of the periodic LPA model. The unstable 2-cycle is not shown. At approximately $\alpha = 0.42$ the attenuant stable cycle and the unstable cycle annihilate each other in a saddle-node bifurcation, while the resonant stable cycle persists for all $\alpha < 1$. The arrows locate the experimental treatments at $\alpha = 0$, $\alpha = 0.40$, and $\alpha = 0.60$. (c) Same as Fig. 1(b) except shown for total population size.

adults. The discrete time interval is 2 weeks. The coefficient $b > 0$ denotes the average number of larvae recruited per adult per unit time in the absence of cannibalism, $0 < \mu_l, \mu_a < 1$ are the larval and adult probabilities of dying from causes other than cannibalism, and the exponentials represent the probabilities that individuals survive cannibalism one unit of time, with 'cannibalism coefficients' $c_{el}, c_{ea}, c_{pa} > 0$.

Model (1) is deterministic. The incorporation of stochastic fluctuations is critical for casting nonlinear population models as testable hypotheses (Dennis *et al*., 1995); nevertheless, stochasticity brings a new layer of conceptual questions. Different types of mechanisms produce different patterns of variability. In particular, two broad classes of stochastic mechanisms important to populations have been widely discussed: environmental stochasticity and demographic stochasticity (May, 1974; Shaffer, 1981). In either case, the stochastic process for the vector N_t of stage numbers can be approximated as a nonlinear autoregressive model of the form

$$X_t = h(X_{t-1}) + E_t$$

where X_t is the vector of state variables (e.g., abundance of the stages, possibly transformed) at time t, the function $h(\cdot)$ is the 'skeleton' (Tong, 1990) representing the deterministic trends that would affect the population in the absence of stochasticity, E_t is a vector random variable having normal distribution with mean zero and variance-covariance matrix Σ, and $E_1, E_2, \ldots$ are uncorrelated. In the case of environmental stochasticity, the transformation $X_t = [lnL_t, lnP_t, lnA_t]'$ is appropriate. In the case of demographic stochasticity, one would use the transformation $X_t = \left[\sqrt{L_t}, \sqrt{P_t}, \sqrt{A_t}\right]'$ for the nonlinear autoregressive model approximation.

Stochastic models have emergent properties that can be substantially different from the deterministic skeleton. Noise continually stirs the system, knocking trajectories away from the attractors of the skeleton. We consider two examples. First, transient phenomena, such as a visitation to the neighborhood of an unstable equilibrium, eventually reoccur. Sometimes an unstable point (or other invariant sets such as an unstable cycle or fractal set) resides on a reduced-dimensional stable manifold, so that trajectories near the manifold tend to move toward the unstable point before diverging toward a stable attractor (Cushing *et al*., 1998). Thus, trajectories in the stochastic system may display occasional 'fly-bys' of repelling regions of phase space, followed by fresh transient returns to the attracting region. Second, populations sometimes exhibit temporal oscillations and often these oscillations shift phase. Henson *et al*. (1998) hypothesized that phase shifts correspond to stochastic jumps between basins of attraction in an appropriate phase space which associates the different phases of a periodic cycle with distinct attractors. Later in this paper (see Section 6.2.3), we shall use a stochastic model and a similar stochastic jump hypothesis to explain the transients observed in the experimental cultures.

The LPA model has been validated by means of a number of experiments, and has been used successfully to predict transitions between equilibria, periodic cy-

cles, invariant loops, and chaos, as well as saddle phenomena and phase switching in population cycles (see Costantino *et al*., 1995, 1997, 1998; Cushing *et al*., 1996, 1998; Dennis *et al*., 1995, 1997; Desharnais *et al*., 1997; Beniot *et al*., 1998; Henson *et al*., 1998).

Henson and Cushing (1997) and Costantino *et al*. (1998) modified the autonomous LPA model (1) to account for the periodic flour volume. Since Jillson alternated the flour between 32 g and 8 g every 2 weeks, we introduced period-2 forcing into the model. In particular, we assumed the cannibalism rates c'_{el}, c'_{ea} and c'_{pa} in the periodically-forced version of the model would be inversely proportional to flour volume $V_t = V_{ave}(1 + \alpha(-1)^t)$ by means of

$$c'_{el} = \frac{c_{el} V_{ave}}{V_t} \qquad c'_{ea} = \frac{c_{ea} V_{ave}}{V_t} \qquad c'_{pa} = \frac{c_{pa} V_{ave}}{V_t} \tag{2}$$

where c_{el}, c_{ea} and c_{pa} are the constant cannibalism rates in the average flour volume V_{ave}, and the parameter $0 < \alpha < 1$ is the relative amplitude of the flour volume oscillation.

This assumption regarding cannibalism rates was mechanistically derived from the fact that cannibalism occurs by random collision between the mobile and immobile life stages, and was supported in laboratory experiments (see Costantino *et al*., 1998).

The periodic LPA model was obtained by utilizing the variable cannibalism rate hypothesis (2) in model (1):

$$\begin{aligned} L_{t+1} &= bA_t \exp\left(\frac{-c_{ea}A_t - c_{el}L_t}{1 + \alpha(-1)^t}\right) \\ P_{t+1} &= (1 - \mu_t)L_t \\ A_{t+1} &= P_t \exp\left(\frac{-c_{pa}A_t}{1 + \alpha(-1)^t}\right) + (1 - \mu_a)A_t \end{aligned} \tag{3}$$

for relative amplitude $0 < \alpha < 1$. When $\alpha = 0$, the periodic LPA model (3) reduces to the autonomous LPA model (1).

We did not directly parametrize the periodic LPA model (3) with data from fluctuating habitats. Instead, we used a parametrization of the autonomous LPA model (1) obtained from a constant habitat historical data set (Costantino *et al*., 1997). Numerical simulations based on this parametrization revealed the existence of robust multiple attracting 2-cycles at increased values of c_{el} and μ_a. Extensive numerical exploration led us to decide to experimentally manipulate or 'target' three parameters

$$c_{ea}^{\text{target}} = 0.01 \qquad c_{el}^{\text{target}} = 0.1 \qquad \mu_a^{\text{target}} = 0.1. \tag{4}$$

The experimental protocol used to obtain the target values is described in detail in Section 5. With the maximum likelihood (ML) parameter estimates

$$b = 6.598, \qquad \mu_l = 0.2055, \qquad \text{and} \qquad c_{pa} = 0.004700 \tag{5}$$

(Costantino *et al*., 1997) and the three target value parameters, the periodic LPA model predicted the multiple attractors as described in the next section.

4. MODEL PREDICTIONS/DESIGN OF EXPERIMENTS

For the parameter values (4) and (5), the LPA model ($\alpha = 0$) predicts a stable 2-cycle whose values are given by the stage vectors (rounded to the nearest beetle)

$$[L_0, P_0, A_0] = [162, 0, 243]$$

$$[L_1, P_1, A_1] = [0, 129, 219].$$

The shift

$$[L_0, P_0, A_0] = [0, 129, 219]$$

$$[L_1, P_1, A_1] = [162, 0, 243]$$

by one time step is also a stable 2-cycle solution. Furthermore, when $\alpha = 0$ the model has an unstable saddle equilibrium

$$[L_e, P_e, A_e] = [23, 19, 110].$$

As $\alpha > 0$ is perturbed away from zero, that is, as habitat periodicity is introduced into the model, the first stable 2-cycle decreases in average, while the second increases in average. These out-of-phase locally stable cycles of greater and smaller averages are henceforth referred to as 'resonant' and 'attenuant' 2-cycles, respectively. The unstable saddle equilibrium becomes an unstable saddle 2-cycle with the introduction of periodic forcing. At $\alpha_0 \simeq 0.42$ the attenuant stable 2-cycle and the unstable 2-cycle annihilate each other in a saddle-node bifurcation, while the resonant stable 2-cycle persists for all $\alpha < 1$ [Fig. 1(b) and (c)].

The model therefore predicts three asymptotic regimes as indexed by the relative amplitude α of the habitat fluctuation: for $\alpha = 0$, the stable cycle and its time shift of opposite phase; for $0 < \alpha < \alpha_0$, the locally stable resonant and attenuant cycles; and for $\alpha > \alpha_0$, the stable resonant cycle.

In the *first experiment* we chose to study three relative amplitudes $\alpha = 0, 0.4$, and 0.6 with initial conditions $[L_{IC}, P_{IC}, A_{IC}] = [150, 200, 150]$ and $[150, 0, 150]$. In the *second experiment*, which is a further experimental evaluation of the geometry of the multiple attractors, we focused on the $\alpha = 0.4$ habitat with initial conditions [92, 0, 142], [120, 0, 80], and [250, 0, 50]. A detailed account of the model's predictions and the design of experiment follows. Tables 1 and 2 summarize the model-predicted asymptotic stage structures according to initial condition and forcing amplitude.

Table 1. The design of the first experiment has two initial stage structures and three flour volume amplitudes. The model-predicted asymptotic stage structures and the assigned replicate labels are given for each of the six treatments.

Relative amplitude, α, of the flour volume, V, oscillation						
Initial stage structure	$\alpha = 0$ $V = 20$ g		$\alpha = 0.4$ $V_t = 28, 12, \ldots$		$\alpha = 0.6$ $V_t = 32, 8, \ldots$	
$L_{IC} = 150$	$L_0 = 162$	$L_1 = 0$	$L_0 = 0$	$L_1 = 227$	$L_0 = 0$	$L_1 = 259$
$P_{IC} = 200$	$P_0 = 0$	$P_1 = 129$	$P_0 = 180$	$P_1 = 0$	$P_0 = 206$	$P_1 = 0$
$A_{IC} = 150$	$A_0 = 243$	$A_1 = 219$	$A_0 = 306$	$A_1 = 340$	$A_0 = 350$	$A_1 = 388$
	[replicates 1,10[a], 14]		[replicates 3, 9[a], 18]		[replicates 4[a], 11, 16]	
$L_{IC} = 150$	same		$L_0 = 92$	$L_1 = 0$	same	
$P_{IC} = 0$	as		$P_0 = 0$	$P_1 = 73$	as	
$A_{IC} = 150$	above		$A_0 = 142$	$A_1 = 128$	above	
	[replicates 6[a], 12, 17]		[replicates 5, 8[a], 13]		[replicates 2[a], 7, 15]	

[a]Replicates continued beyond week 76.

Table 2. The design of the second experiment has three initial stage structures for the alternating habitat with relative amplitude $\alpha = 0.4$. The model-predicted asymptotic stage structures and the assigned replicate labels are given for each of the three treatments.

$L_{IC} = 120$	$L_0 = 92$	$L_1 = 0$
$P_{IC} = 0$	$P_0 = 0$	$P_1 = 73$
$A_{IC} = 80$	$A_0 = 142$	$A_1 = 128$
	[replicates 21, 26, 29, 30]	
$L_{IC} = 250$	$L_0 = 0$	$L_1 = 227$
$P_{IC} = 0$	$P_0 = 180$	$P_1 = 0$
$A_{IC} = 50$	$A_0 = 306$	$A_1 = 340$
	[replicates 24, 25, 28, 31]	
$L_{IC} = 92$	$L_0 = 92$	$L_1 = 0$
$P_{IC} = 0$	$P_0 = 0$	$P_1 = 73$
$A_{IC} = 142$	$A_0 = 142$	$A_1 = 128$
	[replicates 22, 23, 27, 32]	

Note that the orbits of nonautonomous models (of which the periodic LPA model is one) should not be visualized in (L, P, A) phase space since a given point in space can give rise to two different orbits depending on the starting time. However, the first *composite* of the periodic LPA model is autonomous, and its phase portrait facilitates visualization of the model predictions when $\alpha > 0$. The orbits of the composite model correspond to the even time steps $t = 0, 2, 4, \ldots$ of the orbits of the periodically-forced model. We will present periodic LPA model predictions as time series, while the composite predictions (every other step) will be shown in composite phase space.

4.1. ***Constant 20 g habitat*** **($\alpha = 0$).** When $\alpha = 0$, both the initial conditions [150, 200, 150] and [150, 0, 150] give rise to LPA model orbits which approach the 2-cycle

$$[L_0, P_0, A_0] = [162, 0, 243]$$

$$[L_1, P_1, A_1] = [0, 129, 219].$$

L-stage numbers are predicted to oscillate as shown in the LPA model time series in Fig. 2(a).

The composite model has two stable fixed points [162, 0, 243] and [0, 129, 219]. In composite phase space, both orbits of the composite map approach the fixed point [162, 0, 243] of the composite map [Fig. 2(a)].

4.2. ***Alternating 28–12 g habitat*** **($\alpha = 0.4$).** When $\alpha = 0.4$, the periodic LPA model admits a locally stable resonant 2-cycle solution

$$[L_0, P_0, A_0] = [0, 180, 306]$$

$$[L_1, P_1, A_1] = [227, 0, 340],$$

a locally stable attenuant 2-cycle solution

$$[L_0, P_0, A_0] = [92, 0, 142]$$

$$[L_1, P_1, A_1] = [0, 73, 128]$$

of opposite phase, and an unstable saddle 2-cycle solution

$$[L_0, P_0, A_0] = [64, 3, 121]$$

$$[L_1, P_1, A_1] = [4, 51, 111].$$

The resonant and attenuant locally stable 2-cycle solutions and the unstable saddle 2-cycle solution of the periodic LPA model correspond to locally stable 'upper' and 'lower' fixed points [0, 180, 306] and [92, 0, 142], and a saddle fixed point [64, 3, 121] of the composite map. Numerical investigations indicate that the basins of attraction of the two stable fixed points are 'simple'; the boundary is a 'smooth' surface in (L, P, A) space. The saddle lies on the basin boundary, and the stable manifold of the saddle acts as the boundary between the two basins of attraction.

Table 3 lists the eigenvalues and eigenspace basis vectors for the linearizations of the composite map about each of its three fixed points. The linear analysis, coupled with numerical simulations, lead to the following model predictions.

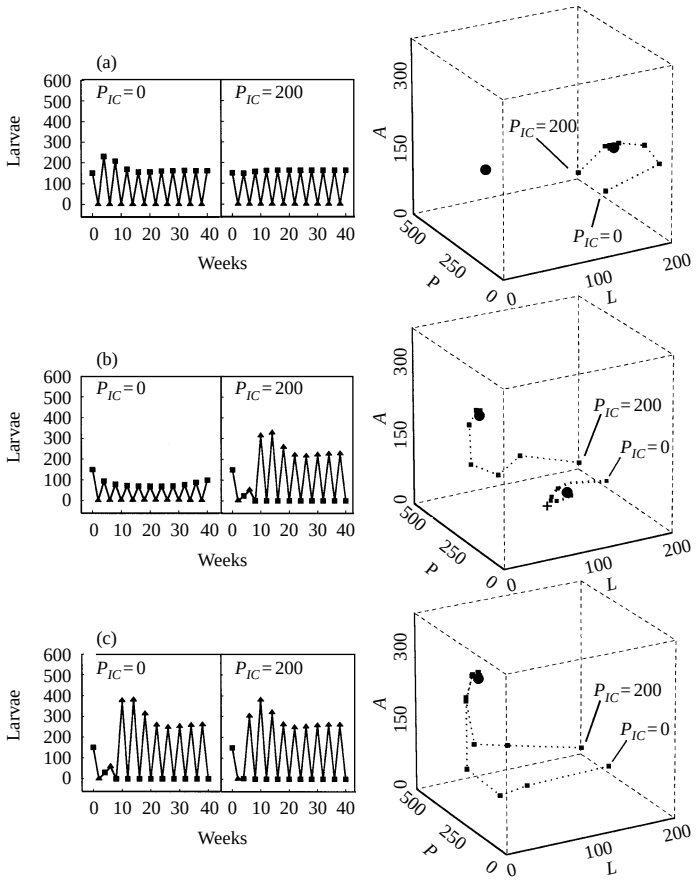

Figure 2. First experiment. Model predictions (including transients) for each of the six treatments in the first experiment, shown in L-stage time series and composite phase space. The squares correspond to times when flour volume is high. The circles in phase space represent equilibria of the first composite map. (a) When $\alpha = 0$, both initial conditions are in the same basin of attraction and lead to a 2-cycle with larvae oscillating in-phase with flour volume. In composite phase space, both orbits tend to the same fixed point. (b) When $\alpha = 0.4$, the initial condition $[150, 200, 150]$ is in the basin of attraction of the resonant 2-cycle, with larvae out-of-phase with the habitat. The initial condition $[150, 0, 150]$ is in the basin of attraction of the attenuant 2-cycle, with larvae oscillating in-phase with the habitat. In composite phase space, the first orbit tends to the upper fixed point, while the second approaches the lower fixed point. (c) When $\alpha = 0.6$, both initial conditions lead to the resonant 2-cycle, with larvae out-of-phase with the habitat. This 2-cycle has the largest average of all. In composite phase space, both orbits approach the (upper) fixed point. At this value of α, the lower fixed point no longer exists.

Table 3. Eigenvalues and eigenspace basis vectors for linearizations of the composite LPA model about its three fixed points.

	Eigenvalues and corresponding eigenspace basis vectors
[0.00, 180.36, 305.91]	$\lambda = 0$; [0.03, 1.00, −0.53]
	$\lambda = 0.31 \pm 0.36i$; [0.00, 0.00, 1.00], [0.00, 1.00, −0.44]
[92.29, 0.37, 142.33]	$\lambda = 1.23 \times 10^{-5}$; [0.00, 1.00, −0.69]
	$\lambda = 0.57 \pm 0.44i$; [1.00, −0.04, 0.25], [−0.76, −0.01, 1.00]
[63.60, 2.84, 120.79]	$\lambda = 2.66$; [1.00, −0.08, 0.15]
	$\lambda = 0.70$; [0.23, −0.06, 1.00]
	$\lambda = -1.87 \times 10^{-4}$; [−0.01, 1.00, −0.74]

In the first experiment, the initial conditions [150, 200, 150] and [150, 0, 150] were chosen in the basins of attraction of the resonant and attenuant stable 2-cycles, respectively. Figure 2(b) presents the L-stage periodic LPA model time series predictions for these initial conditions. The orbit originating at [150, 200, 150] oscillates out-of-phase with the habitat (i.e., high L-stage numbers in low flour volume) and attains a larger average, while the orbit starting at [150, 0, 150] oscillates in-phase with the habitat (i.e., high L-stage numbers in high flour volume) and has a depressed average.

In the context of the composite model, these initial conditions are in the basins of the upper and lower stable fixed points, respectively. Figure 3(a) presents the three fixed points of the composite map, the basin boundary, and the composite model orbits generated by the two initial conditions of the first experiment. The orbit starting with initial condition [150, 200, 150] quickly approaches the $L = 0$ plane, and then spirals more slowly into the upper fixed point. The orbit does not approach the lower fixed point or the saddle. The orbit with initial condition [150, 0, 150], however, experiences the influence of the stable manifold of the saddle. It follows the basin boundary and flies by the saddle before moving to approximately the $P = 0.37$ plane and spiraling into the lower fixed point.

In the second experiment, the initial condition [92, 0, 142] was placed directly on the model-predicted attenuant 2-cycle, and so experimental cultures initiated at [92, 0, 142] are predicted to remain on the attenuant 2-cycle. The initial condition [250, 0, 50] was placed in the basin of attraction of the resonant 2-cycle, but close to the boundary basin. In composite phase space, the model orbit flies around the basin boundary and by the saddle before approaching the $L = 0$ plane and spiraling into the upper fixed point [Fig. 3(b)]. The initial condition [120, 0, 80] was placed in the basin of the attenuant cycle. In composite phase space, the model orbit spirals into the lower fixed point as show in Fig. 3(b).

4.3. ***Alternating 32–8 g habitat*** **($\alpha = 0.6$).** When $\alpha = 0.6$, both the initial conditions [150, 200, 150] and [150, 0, 150] give rise to periodic LPA model orbits which approach the resonant 2-cycle

$$[L_0, P_0, A_0] = [0, 206, 350]$$

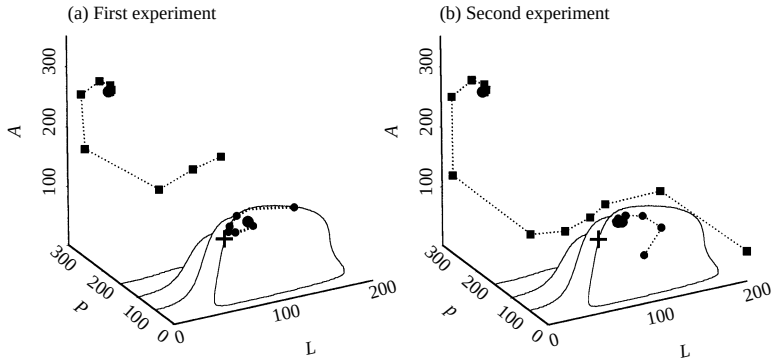

Figure 3. Model predictions for the composite periodic LPA model with $\alpha = 0.4$, shown in composite phase space. The large circles represent the two equilibria of the composite map. The saddle fixed point (cross) lies on the basin boundary. (a) First experiment. The orbit starting at [150, 200, 150] (squares) tends to the upper fixed point. The orbit starting at [150, 0, 150] (small circles) follows the basin boundary, flies by the saddle, then approaches the lower fixed point. (b) Second experiment. The orbit starting at [250, 0, 50] (squares) follows the boundary and flies by the saddle before approaching the upper fixed point. The orbit starting at [120, 0, 80] (small circles) spirals into the lower fixed point.

$$[L_1, P_1, A_1] = [259, 0, 388].$$

L-stage numbers are predicted to oscillate out-of-phase with the habitat and attain the largest average [Fig. 2(c)].

In composite phase space, both orbits of the composite map approach the fixed point [0, 206, 350] of the composite map [Fig. 2(c)].

5. EXPERIMENTAL PROTOCOL

The $\alpha = 0$ or constant 20 g habitat is commonly used in our laboratory and the projected 2-cycles are well documented (Moffa and Costantino, 1977; Desharnais and Costantino, 1980; Jillson, 1980; Costantino *et al.*, 1995, 1997). The $\alpha = 0.6$ alternating 32–8 g habitat was used in the experiment conducted by Jillson (1980) and recently analysed by Henson and Cushing (1997) and Costantino *et al.* (1998). Our design of experiment includes treatments at both $\alpha = 0$ and $\alpha = 0.6$ as controls. The $\alpha = 0.4$ alternating 28–12 g habitat sequence admits the multiple attractors and is the centerpiece of the experiments reported in this paper.

The mathematical analysis of the periodic LPA model was the guide to the conduct of the experiments. In the first experiment, we tested the model predictions at $\alpha = 0$ and $\alpha = 0.6$, and in particular, tested the multiple attracting 2-cycle predic-

tion at $\alpha = 0.4$, using the two initial conditions [150, 200, 150] and [150, 0, 150] (as identified in the previous section) for each of the three habitat regimes. There were three replicates in each of the six treatments for a total of 18 cultures. The RR strain of *Tribolium castaneum* Herbst was used. The animals were held in 120 ml sample bottles and maintained in a dark incubator at 31°C. All cultures were counted every 2 weeks for a total of 76 weeks. Some cultures were discontinued at week 76 while others were maintained through week 140. Following census, and the appropriate experimental manipulation, all of the animals (except eggs) were placed in new media and returned to the incubator.

In the second experiment, which followed the first experiment, we initiated three more treatments in the 28–12 g habitat ($\alpha = 0.4$) with the initial conditions [120, 0, 80], [92, 0, 142], and [250, 0, 50]. Each treatment in the second experiment consisted of four replicates for a total of 12 new cultures. The experimental protocol remained the same. The second study ran for 64 weeks.

The target value for the adult-on-egg cannibalism rate was $c_{ea}^{\text{target}} = 0.010$ [see (4)], while the maximum likelihood (ML) parameter estimate was $c_{ea} = 0.01211$. Therefore, the target value may be written as $c_{ea}^{\text{target}} = c_{ea} + g = 0.01211 - 0.00211$. Similarly, the target value for the larva-on-egg cannibalism rate was $c_{el}^{\text{target}} = 0.10$, while the parameter estimate was $c_{el} = 0.01199$, producing the decomposition $c_{el}^{\text{target}} = c_{el} + h = 0.01199 + 0.08801$. [Note that the ML parameter estimates given above of $c_{ea} = 0.01211$ and $c_{el} = 0.01199$ were the best available at the start of the experiment. These estimates differ slightly from the values $c_{ea} = 0.01155$ and $c_{el} = 0.01209$ given in Costantino *et al.* (1997).]

At the estimated values of c_{ea} and c_{el}, the model predicts

$$L_{t+1}^{\text{predicted}} = bA_t \exp\left(\frac{-c_{ea}A_t - c_{el}L_t}{1 + \alpha(-1)^t}\right)$$

new larvae at time $t + 1$, where L_t and A_t are the numbers of larvae and adults counted at time t, respectively. At the target values of c_{ea}^{target} and c_{el}^{target}, the model predicts

$$\begin{aligned} L_{t+1}^{\text{target}} &= bA_t \exp\left(\frac{-c_{ea}A_t - c_{el}L_t}{1 + \alpha(-1)^t}\right) \exp\left(\frac{-gA_t - hL_t}{1 + \alpha(-1)^t}\right) \\ &= (L_{t+1}^{\text{predicted}}) \exp\left(\frac{0.00211A_t - 0.08801L_t}{1 + \alpha(-1)^t}\right) \end{aligned}$$

new larvae at time $t + 1$.

We manipulated the egg cannibalism rates at their target values by manipulating larval recruitment. If $L_{t+1}^{\text{observed}}$ larvae were counted at time $t + 1$, then the number of larvae L_{t+1} returned to the culture after the $t + 1$ census was computed with the equation

$$L_{t+1} = (L_{t+1}^{\text{observed}}) \exp\left(\frac{0.00211A_t - 0.08801L_t}{1 + \alpha(-1)^t}\right).$$

The exponential factor was the adjustment made to the observed number of larvae at time $t + 1$. Both the number of adults and larvae at time t were part of this calculation. Note that the adjustment factor could result in an increase or decrease in the observed larvae at time $t + 1$. Suppose, for example, $\alpha = 0.4$ with $L_t = 65$, $P_t = 2$, and $A_t = 139$ beetles counted in the 28 g habitat. Then the larval adjustment factor is 0.0207. If at the following census the observed number of L-stage animals were 49, then the number of small larvae returned to the culture would be $(49)(0.0207) = 1$ larva. Since we knew the adjustment factor from the data at time t, laboratory preparations could be made to have L-stage animals available at time $t + 1$.

The target value of the adult death rate was $\mu_a^{\text{target}} = 0.10$. This adult death rate is similar to that observed in unmanipulated laboratory cultures of beetles (Dennis *et al*., 1995). To realize this value, adult mortality was manipulated by removing or adding adults at the time of a census to make the total number of adults that died during the interval (adjusted for the number of natural deaths) equal to 10% of the adults alive at time t. To counter the possibility of genetic changes in life-history characteristics, beginning at week 4 and continuing every month thereafter, the adults returned to the populations after the census were obtained from separate stock cultures maintained under standard laboratory conditions.

Following a census, the animals were placed in 120 ml sample bottles with the 'volume' of standard media allocated by weight: with $\alpha = 0$ a constant 20 g, with $\alpha = 0.4$ an alternating sequence of *initially 28 g* then 12 g, and with $\alpha = 0.6$ an alternating sequence *starting with 32 g* followed by 8 g of media.

6. Results of the First Experiment

We now turn our attention to a comparison of the model predictions and the data. It is important to note that *the model was not re-parametrized* with the new data. Indeed, the new data are compared to predictions based on the parameters (4) and (5) estimated from an independent historical data set. While it is true that L-stage recruitment was manipulated so as to attain 'target' values of c_{ea} and c_{el}, the amount of manipulation necessary was calculated using the parameter values from the independent data set. Thus, the results have in no way been enhanced by 'model fitting', but rather represent the empirical test of predictions of the periodic LPA model.

6.1. ***Constant 20 g habitat*** **($\alpha = 0$).** The observed L-stage time series of 140 weeks for two representative replicates in the constant 20 g habitat are given in Fig. 4(a) and (b). Larval numbers oscillated as predicted by the model in Fig. 2(a).

Figure 4(a) and (b) also present every other census triple $[L, P, A]$ in composite phase space. In this context the two solid circles represent the two stable predicted fixed points [162, 0, 243] and [0, 129, 219] of the composite LPA model. The data

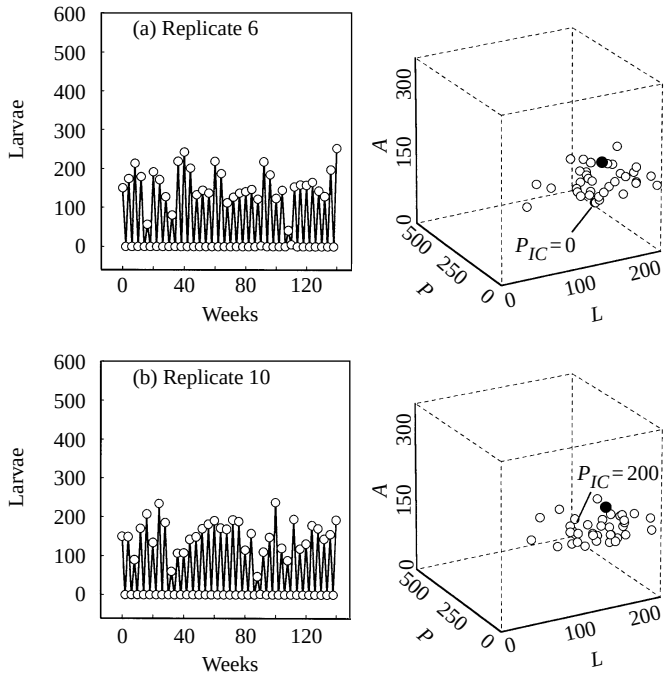

Figure 4. Larval time series data and composite phase space plots for two replicates with different initial conditions but cultured in the constant 20 g habitat, $\alpha = 0$. In the composite map the two full circles are the stable fixed points. (a) Replicate #6 had an initial stage structure of $[L, P, A] = [150, 0, 150]$. (b) Replicate #10 had an initial stage structure of $[L, P, A] = [150, 200, 150]$. Both time series are for 140 weeks.

cluster around the fixed point [162, 0, 143] as forecast in Fig. 2(a).

6.2. ***Alternating 28–12 g habitat*** **($\alpha = 0.4$).** For the intermediate habitat sequence of 28–12 g, the periodic LPA model predicts a 2-cycle of depressed average as well as an opposite phase 2-cycle of enhanced average. We examine each local attractor in turn.

6.2.1. *Stable resonant 2-cycle.* Figure 5 displays the L-stage time series data for the three replicates cultured in the 28–12 g habitat, and started in the basin of attraction of the resonant 2-cycle. L-stage numbers in all three replicates are consistent with the periodic LPA model predictions of Fig. 2(b) by: (1) displaying the predicted transient pattern seen in the first 10 weeks; (2) oscillating out-of-phase with the habitat; and (3) having an average larger than that of the cultures in the constant habitat.

The corresponding composite phase space plots are placed opposite the L-stage time series in Fig. 5. The three cultures proceed directly to the $L = 0$ plane

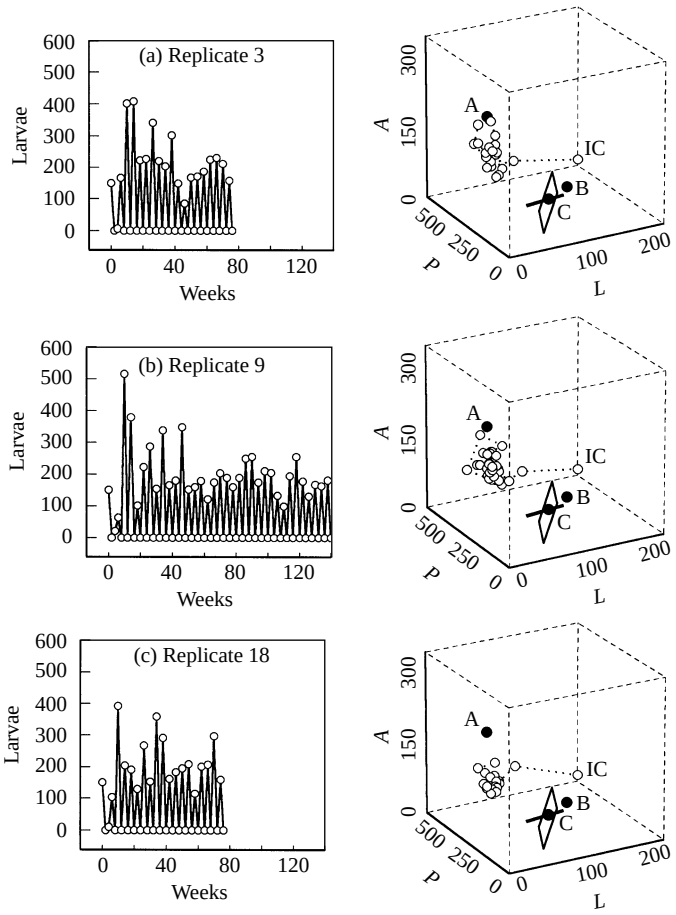

Figure 5. Larval time series data and composite phase space plots for the three replicates cultured in the 28–12 g habitat, $\alpha = 0.40$, and started in the basin of attraction of the resonant 2-cycle at $[L, P, A] = [150, 200, 150]$. The first composite map has two locally stable fixed points (full circles labeled A and B) and an unstable saddle fixed point (full circle labeled C) with a strongly repelling unstable manifold (solid line) and a two-dimensional stable manifold (rectangle) which lies on the basin boundary.

as predicted, where they oscillate in the vicinity of the upper fixed point of the composite map. There was no evidence of any trend toward the lower fixed point. Note that our parameters, obtained as they were from independent historical data, do not predict well the exact location of the upper fixed point.

6.2.2. *Stable attenuant 2-cycle.* Figure 6 displays the L-, P- and A-stage time series data for the three replicates cultured in the 28–12 g habitat, and started in the basin of attraction of the attenuant 2-cycle. The composite phase space plots

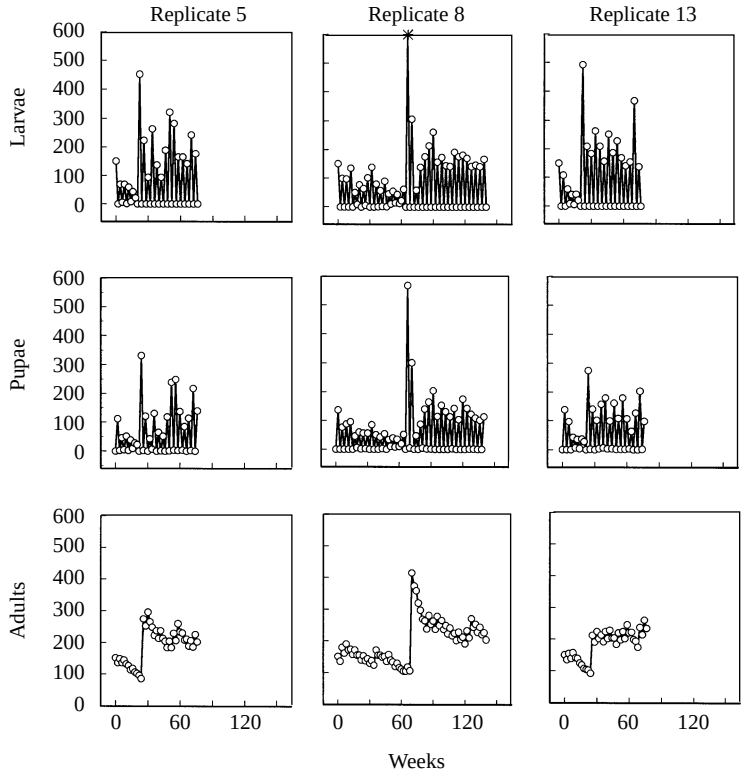

Figure 6. Time series data for the three replicates cultured in the 28–12 g habitat, $\alpha = 0.40$, and started in the basin of attraction of the attenuant 2-cycle at $[L, P, A] = [150, 0, 150]$. Replicates #5 and #13 (with a time series length of 76 weeks) remained close to the lower attractor until week 22 when L-stage numbers of 452 and 493, respectively, clearly marked the transition to the resonant 2-cycle attractor. Replicate #8 (with a time series length of 140 weeks) remained near the attenuant 2-cycle until week 66 when L-stage numbers were 612 (star).

of each replicate are shown in Fig. 7. The three cultures displayed the expected pattern in L-stage numbers [see Fig. 2(b)] for the first 14 weeks. The cultures were *in-phase* with the habitat which means that high numbers of L-stage animals were observed when the cultures were placed into the (high) 28 g habitat.

During weeks 16 to 20 unanticipated observations were recorded. In two replicates the relationship of high larval numbers in the high volume habitat was reversed by week 20. In the third replicate the pattern was altered at week 62.

The reversal of phase is recorded in the data (Figs 6 and 7). At week 16, in both replicates #5 and #13, a modest change from the model prediction was seen: L-stage numbers were smaller in the 28 g habitat than recorded earlier in the time series. Two weeks later (week 18), L-stage numbers which were predicted to be

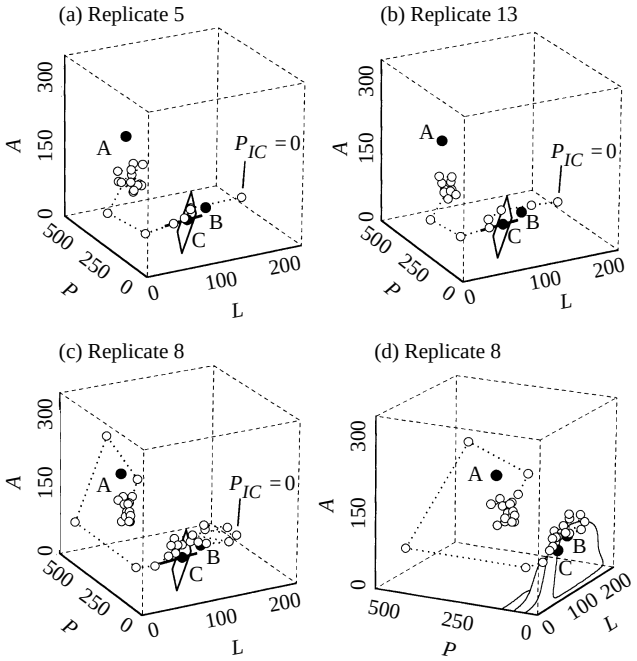

Figure 7. Composite phase space plots of the data (open circles) of the three replicates which were started in the basin of attraction of the lower fixed point. The first composite map has two locally stable equilibria (full circles labeled A and B) and an unstable equilibrium (full circle labeled C) with a strongly repelling unstable manifold (solid line) and a two-dimensional stable manifold (rectangle) which lies on the basin boundary. (a) Replicate #5. (b) Replicate #13. (c) and (d) Two perspectives of composite phase space of the replicate #8 data.

very small (0, 1 or 2 animals) in the 12 g habitat were 22 and 21, respectively. At week 20 the change in the association between L-stage numbers and habitat size had occurred. In the 28 g habitat, rather than the forecast of approximately 70 L-stage animals these replicates each had a single larva. At week 22, large cohorts of L-stage beetles were recorded in both replicates (452 and 493, respectively), followed 2 weeks later by an increase in P-stages and then 2 weeks later adult numbers increased to 274 and 212 beetles, respectively. The cultures were now out-of-phase with the habitat. Both replicates #5 and #13 had moved to the resonant attractor.

On the other hand, replicate #8 stayed near the attenuant 2-cycle until week 62 when a pattern similar to that just described occurred (Figs 6 and 7). At week 70, replicate #8 had 414 adults: a fourfold increase over the number of adults at week 68.

6.2.3. *Stochastic jumps between basins of attraction.* The sudden time series shift observed in all three replicates initialized in the basin of attraction of the attenuant cycle is predicted by a stochastic version of the periodic LPA model. Note that, in composite phase space, replicates #5 and #13 flew by the saddle [as predicted by the deterministic model, Fig. 3(a)], but then quickly escaped along the unstable manifold of the saddle to finally oscillate in the $L = 0$ plane (Fig. 7). Replicate #8 lingered near the lower fixed point and the saddle much longer before following this pattern (Fig. 7). We hypothesize that each replicate, at different times in their histories, was stochastically 'bumped' into the basin of attraction of the resonant cycle. In composite phase space, this is equivalent to replicates stochastically 'jumping' from the basin of the lower fixed point of the composite map into the basin of the upper fixed point.

To investigate this hypothesis we introduce a *stochastic* periodic LPA model:

$$\begin{aligned} L_{t+1} &= bA_t \exp\left(\frac{-c_{ea}A_t - c_{el}L_t}{1+\alpha(-1)^t} + E_{1t}\right) \\ P_{t+1} &= L_t(1-\mu_l)\exp(E_{2t}) \\ A_{t+1} &= \left[P_t \exp\left(\frac{-c_{pa}A_t}{1+\alpha(-1)^t}\right) + (1-\mu_a)A_t\right]\exp(E_{3t}). \end{aligned}$$

The variables E_{1t}, E_{2t}, and E_{3t} are random noise variables having a multivariate normal distribution with mean zero and variance-covariance matrix

$$\sum = \begin{pmatrix} 0.3411 & 0.0731 & -0.0017 \\ 0.0731 & 0.2488 & 0.0003 \\ -0.0017 & 0.0003 & 0.0002 \end{pmatrix}$$

estimated simultaneously with the parameters obtained from historical constant habitat data [see (4) and (5)]. The noise variables represent the unpredictable departures of the observations from the deterministic skeleton due to *environmental* causes.

The attenuant attractor of the deterministic periodic LPA model is locally stable. However, *stochastic* model orbits starting in the basin of attraction of the attenuant attractor eventually move to the resonant attractor. For example, in Fig. 8(a) a stochastic orbit started at the experimental initial condition $[150, 0, 150]$ jumps into the basin of the resonant attractor at week 20 with a pattern similar to that of replicates #5 and #13 (Figs 6 and 7). Another stochastic realization [Fig. 8(b)] jumps basins at week 62; compare this behavior with that of replicate #8 (Figs 6 and 7).

One might expect the stochastic orbits eventually to return to the attenuant attractor, and so on. Interestingly, however, in 50 000 stochastic simulations, orbits arriving (or starting) in the basin of the resonant attractor *never* moved to the attenuant attractor. We will explore this phenomenon in detail in another paper.

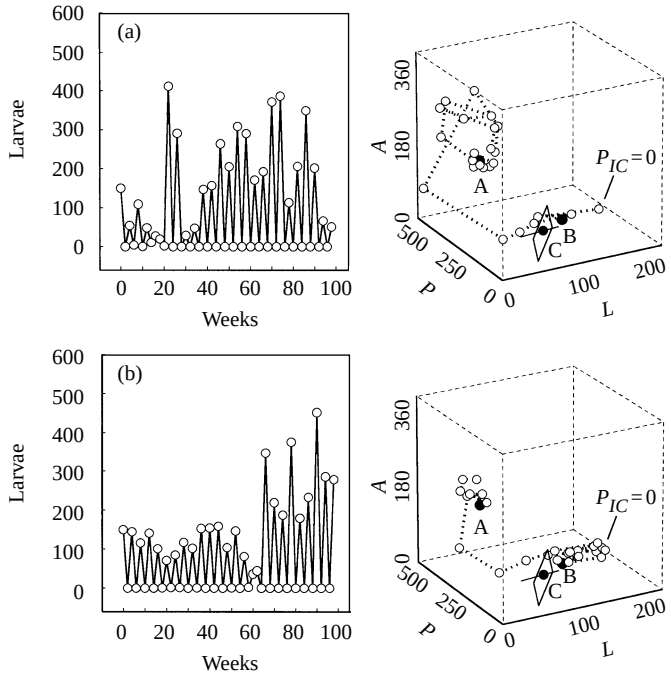

Figure 8. Larval time series and phase space plots of two stochastic periodic model orbits in the 28–12 g habitat, $\alpha = 0.40$, with the initial condition $[L, P, A] = [150, 0, 150]$. (a) An orbit that changes its phase to the resonant cycle at week 20. (b) A model orbit that 'jumps' stochastically to the resonant attractor at week 62.

How long does it take for a stochastic orbit initialized in the basin of the attenuant attractor to move to the resonant attractor? Figure 9 presents a frequency histogram of 'jump times' calculated from 50 000 stochastic orbits. The 'jump time' in these calculations is the time at which the orbit first changes its phase from that of the attenuant 2-cycle to that of the resonant 2-cycle. The mean jump time is 18.55 weeks which is close to the jump time of replicates #5 and #13. Although replicate #8, with its jump time of 62 weeks, provides strong evidence for the existence of the attenuant 2-cycle, it is seen from the model's point of view as an outlier. Note that *all* of the 50 000 model orbits moved to the resonant cycle by week 96.

6.3. ***Alternating 32–8 g habitat*** **($\alpha = 0.6$).** The observed L-stage time series of 140 weeks for two representative replicates in the alternating 32–8 g habitat are given as time series in Fig. 10. Both initial stage structures led to beetle numbers which oscillated out-of-phase with the habitat, as predicted in Fig. 2(c). The average total population sizes were larger than the average total population sizes in the other habitat sequences, as predicted by the model. However, the model predicted an average total population size of 602 animals, while the six replicates averaged

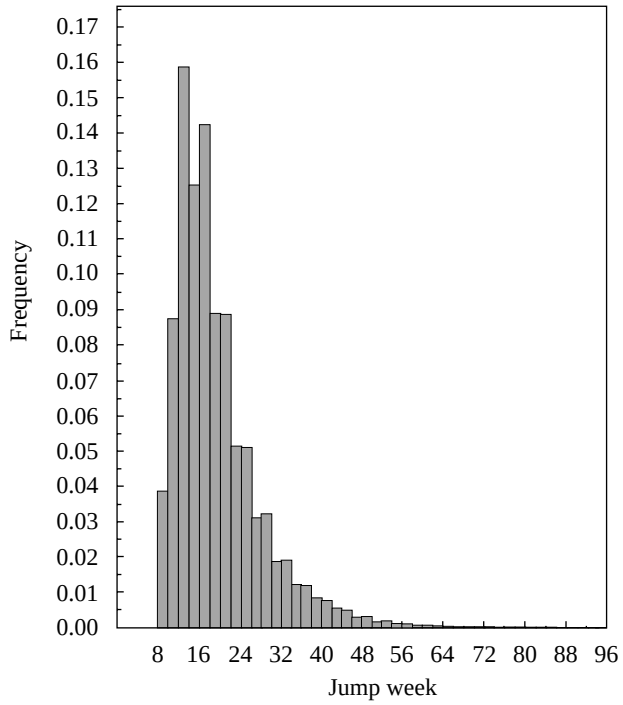

Figure 9. Frequency histogram of the 'jump times' calculated from 50 000 stochastic orbits started at the initial condition in the experiment for the attenuant attractor ($[L, P, A] = [150, 0, 150]$). Mean jump time was 18.55 weeks.

472 animals after the removal of 4 weeks of transients. Note that the L-stage numbers in both replicates #2 and #4 follow the transient patterns predicted in Fig. 2(c).

Composite phase space plots of the $[L, P, A]$ triples from replicates #2 and #4 are also presented in Fig. 10. The predicted 2-cycle of the periodic LPA model appears as a fixed point of the composite map. Again, the even time data cluster below the predicted fixed point attractor.

7. Results of the Second Experiment

The second experiment was conducted to further clarify the geometry of the multiple attractors when $\alpha = 0.4$. Beetle cultures were placed at three different initial conditions in the alternating 28–12 g habitat. In Fig. 3(b) the model-predicted deterministic orbits for each initial condition appear in composite phase space.

7.1. = [250, 0, 50]]Initial condition [*L, P, A*] = [250, 0, 50]. Figure 11 shows the composite phase space plots for each of the four replicate cultures started in the basin of attraction of the resonant attractor but far from the final state. Each

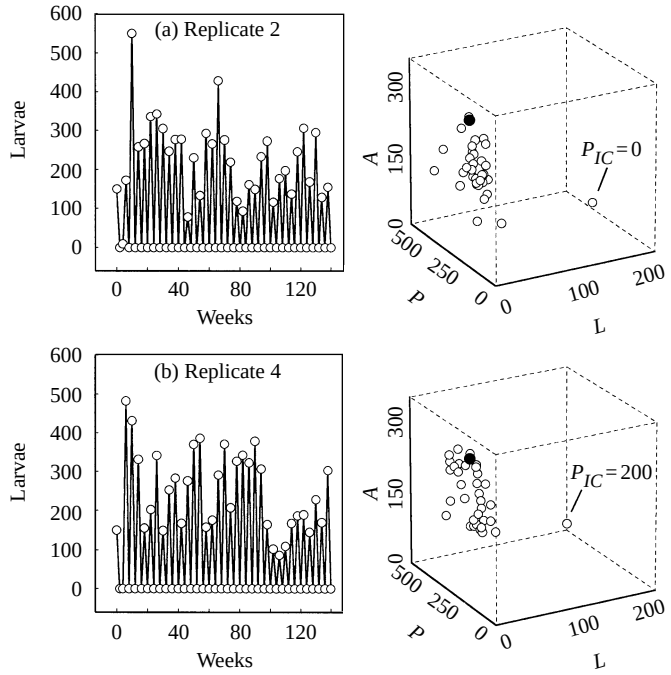

Figure 10. Larval time series data and composite phase space plots for two replicates with different initial conditions but cultured in the 32–8 g habitat, $\alpha = 0.60$. The full circle in composite phase space represents the equilibrium of the first composite map. (a) Replicate #2 had an initial stage structure of $[L, P, A] = [150, 0, 150]$. (b) Replicate #4 had an initial stage structure of $[L, P, A] = [150, 200, 150]$. Both time series are for 140 weeks.

culture moved around the basin boundary of the two attractors and then toward the forecast final state. The patterns displayed by the experimental cultures were remarkably similar to the deterministic model-predicted pattern [see Fig. 3(b)]. Note that replicate #31 [Fig. 11(d)] moved past the lower attractor as predicted, but looped back toward the basin separatrix before going to the final state. In the entire project, no culture started in the basin of the resonant cycle moved to the attenuant cycle. The 'loop' observed in replicate #31 was as close as any culture came to moving from the resonant to the attenuant attractor.

7.2. = [120, 0, 80]]Initial condition [*L, P, A*] = [120, 0, 80]. Cultures started with 120 larvae, 0 pupa, and 80 adults were predicted to be *in* the basin of attraction of the attenuant attractor and therefore were expected to approach that attractor. As noted in the composite phase space plots in Fig. 12, this was not observed. The final state of all four replicates was the resonant attractor. However, the replicates took different routes to the final state. Replicates #26 and 29 [Fig. 12(b) and (c)]

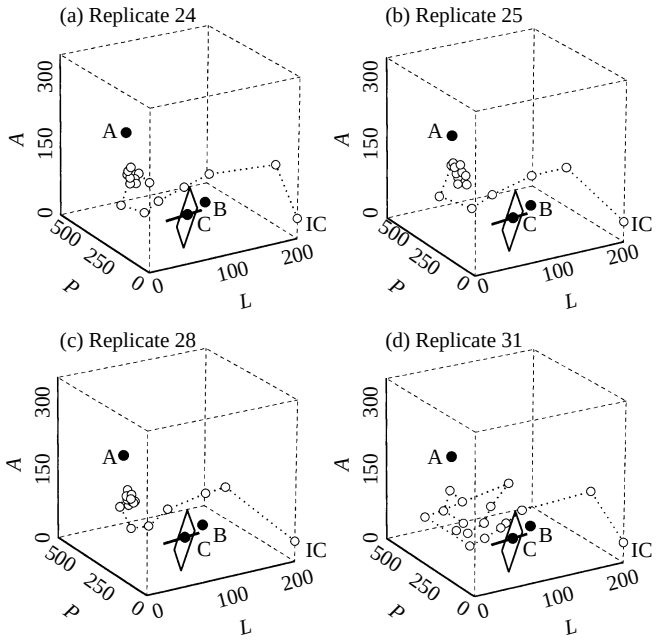

Figure 11. Composite phase space plots of the data from the four replicates in the second experiment which were started in the basin of the upper fixed point at $[L, P, A] = [250, 0, 50]$.

were apparently pushed stochastically very early (week 20) into the basin of the resonant cycle and then the cultures followed a path quite similar to that noted for the replicates initiated with $L = 250$, $P = 0$, $A = 50$ (see Fig. 11). On the other hand, replicate #21 stayed close to the attenuant cycle for 40 weeks while replicate #30 remained close to the predicted attractor for 52 weeks [Fig. 12(a) and (d)].

7.3. = [92, 0, 142]]Initial condition [*L, P, A*] = [92, 0, 142]. The initial condition $L = 92$, $P = 0$, $A = 142$ placed the cultures directly *on* the model-predicted attenuant cycle. The deterministic forecast is that the cultures will *remain* on the attractor. As seen in Fig. 13, three of the four replicates moved off the attractor quickly (week 20 approximately). Once off the attractor, replicates #22, 23 and 27 followed the model-predicted orbit to the resonant attractor. Replicate #32 [Fig. 13(d)] did hover about the attenuant attractor for 48 weeks before following a now familar path to the resonant attractor.

8. DISCUSSION

Nearly 40 years ago, the *idea* that populations might resonate in response to environmental fluctuations was stated by Slobodkin (1961, p. 155): '... populations are

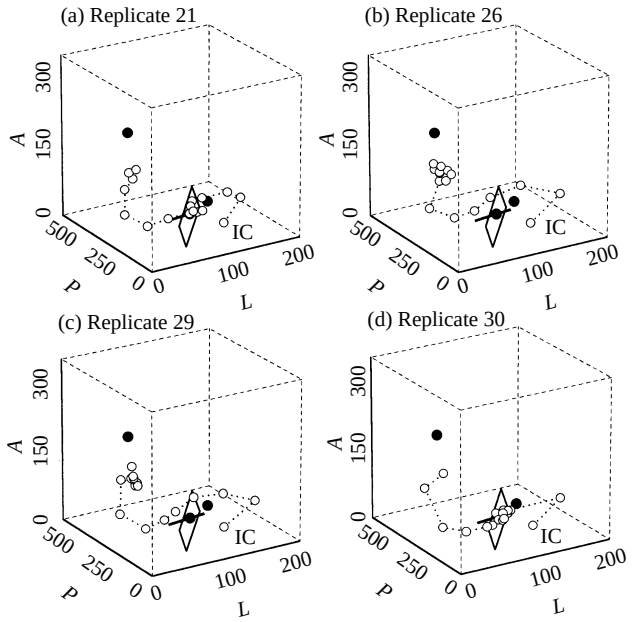

Figure 12. Composite phase space plots of the data from the four replicates in the second experiment which were started in the basin of the lower fixed point at $[L, P, A] = [120, 0, 80]$.

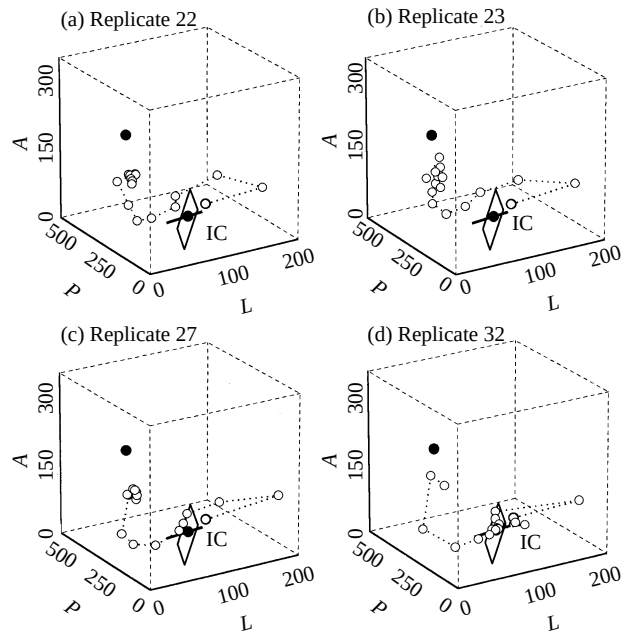

Figure 13. Composite phase space plots of the data from the four replicates in the second experiment which were started on the lower fixed point at $[L, P, A] = [92, 0, 142]$.

feedback systems and that any such systems will of necessity act as a resonator, selectively responding to the fluctuations in the environment according to their time periodicity, the primary resonance being in the period of approximately one generation. The most obvious test of this concept will be a direct laboratory study in a controlled environment'. Aware of Slobodkin's speculation, Oster and Takahashi (1974) added an analysis of a mathematical model that confirmed the possibility of resonant cycles. Unaware of Slobodkin's comment, Jillson (1980) conducted a needed 'laboratory study'.

As noted in the Introduction, the periodic LPA model was used in Costantino *et al*. (1998) to explain the increased average biomass observed in the 32–8 g habitat of the Jillson (1980) experiment as a type of resonance phenomenon in which the inherent biological oscillation resonates with the periodic habitat. The intervals of large flour volume with reduced cannibalism rates boost the larval recruitment rate, while the intervals of small flour volume with increased cannibalism rates depress the larval recruitment rate. This explanation also holds for the stable resonant 2-cycle of enhanced average predicted (and now observed) in the intermediate 28–12 g habitat. However, the model prediction of the stable attenuant 2-cycle of depressed average in the 28–12 g habitat sequence came as something of a surprise, and presented us with an excellent opportunity for further experimentation.

The treatments placed in the previously studied 20 g constant habitat and 32–8 g habitat regimes were 'controls' for our investigation of the 28–12 g habitat. We viewed the resonant and attenuant locally stable 2-cycles predicted in the 28–12 g habitat as multiple attractors and started treatments in each basin of attraction. Fortunately, the basins were 'simple', with 'smooth' boundaries; had they been been riddled or marbled with fractal boundaries, stochastic effects might have made it impossible to locate the multiple attractors (Nusse and Yorke, 1996; Neubert, 1997). Furthermore, the predicted cycles differed not only in average, but also in phase thus increasing the possibility of unambiguous empirical detection.

The data from the intermediate 28–12 g habitat treatments evidenced the existence of the resonant and attenuant 2-cycles, as well as the saddle cycle, with transient behavior conforming to the linearized predictions of Section 4.2. The data from the 'bracketing' treatment regimes of constant 20 g and 32–8 g habitats also displayed the features of the model predictions.

We determined that habitat periodicity can lead to multiple attracting states in population numbers, and that the advent of environmental fluctuation can enhance *or depress* average population numbers. In particular, habitat periodicity in this experiment led to multiple stable 2-cycles of enhanced and depressed average. It was also clear that natural stochasticity combined with the effects of an unstable 'saddle cycle' separating the two stable cycles greatly influenced the transients and final states of the experimental populations. Thus, in experimental regimes containing multiple attractors, the presence of unstable invariant sets, as well as stochasticity and the nature, location, and size of basins of attraction, are all central to the interpretation of data.

ACKNOWLEDGEMENTS

This research was supported in part by U.S. National Science Foundation grants DMS-9625576 and DMS-9616205. Henson was supported by an American Fellowship from the American Association of University Women Educational Foundation.

REFERENCES

Beniot, H. P., E. McCauley and J. R. Post (1998). Testing the demographic consequences of cannibalism in *Tribolium confusum*. *Ecology* **79**, 2839–2851.

Costantino, R. F., J. M. Cushing, B. Dennis and R. A. Desharnais (1995). Experimentally induced transitions in the dynamic behavior of insect populations. *Nature* **375**, 227–230.

Costantino, R. F., J. M. Cushing, B. Dennis, R. A. Desharnais and S. M. Henson (1998). Resonant population cycles in alternating habitats. *Bull. Math. Biol.* **60**, 247–273.

Costantino, R. F., R. A. Desharnais, J. M. Cushing and B. Dennis (1997). Chaotic dynamics in an insect population. *Science* **275**, 389–391.

Cushing, J. M., B. Dennis, R. A. Desharnais and R. F. Costantino (1996). An interdisciplinary approach to understanding non-linear ecological dynamics. *Ecol. Model.* **92**, 111–119.

Cushing, J. M., B. Dennis, R. A. Desharnais and R. F. Costantino (1998). Moving toward an unstable equilibrium: saddle nodes in population systems. *J. Anim. Ecol.* **67**, 298–306.

Dennis, B., R. A. Desharnais, J. M. Cushing and R. F. Costantino (1995). Non-linear demographic dynamics: mathematical models, statistical methods, and biological experiments. *Ecol. Monogr.* **65**, 261–281.

Dennis, B., R. A. Desharnais, J. M. Cushing and R. F. Costantino (1997). Transitions in population dynamics: equilibria to periodic cycles to aperiodic cycles. *J. Anim. Ecol.* **66**, 704–729.

Desharnais, R. A. and R. F. Costantino (1980). Genetic analysis of a population of *Tribolium*. VII. Stability: response to genetic and demographic perturbations. *Can. J. Genetics Cytol.* **22**, 577–589.

Desharnais, R. A., R. F. Costantino, J. M. Cushing and B. Dennis (1997). Estimating chaos in an insect population. *Science* **276**, 1881–1882.

Henson, S. M. (1999). Multiple attractors and resonance in periodically-forced population models, (Submitted.)

Henson, S. M. and J. M. Cushing (1997). The effect of periodic habitat fluctuations on a non-linear insect population model. *J. Math. Biol.* **36**, 201–226.

Henson, S. M., J. M. Cushing, R. F. Costantino, B. Dennis and R. A. Desharnais (1998). Phase switching in population cycles. *Proc. R. Soc. Lond. B* **265**, 2229–2234.

Jillson, D. (1980). Insect populations respond to fluctuating environments. *Nature* **288**, 699–700.

May, R. M. (1974). Biological populations with non-overlapping generations: stable points, stable cycles, and chaos. *Science* **186**, 645–647.

May, R. M. (1977). Thresholds and breakpoints in ecosystems with a multiplicity of stable states. *Nature* **269**, 471–477.

Moffa, A. M. and R. F. Costantino (1977). Genetic analysis of a population of *Tribolium.* VI. Polymorphism and demographic equilibrium. *Genetics* **87**, 785–805.

Neubert, M. G. (1997). A simple population model with qualitatively uncertain dynamics. *J. Theor. Biol.* **189**, 399–411.

Nisbet, R. M. and W. S. C. Gurney (1981). *Modelling Fluctuating Populations*, New York: Wiley and Sons.

Nusse, H. E. and J. A. Yorke (1996). Basins of attraction. *Science* **271**, 1376–1380.

Oster, G. and Y. Takahashi (1974). Models for age-specific interactions in a periodic environment. *Ecol. Monogr.* **44**, 483–501.

Park, T., M. Nathanson, J. R. Ziegler and D. B. Mertz (1970). Cannibalism of pupae by mixed-species populations of adult *Tribolium*. *Physiol. Zool.* **43**, 166–184.

Petraitis, P. S. and R. E. Latham (1999). The importance of scale in testing the origins of alternative community states. *Ecology* **80**, 429–442.

Renshaw, E. (1991). *Modelling Biological Populations in Space and Time*, Cambridge: Cambridge University Press.

Shaffer, M. L. (1981). Minimum population sizes for species conservation. *Bioscience* **31**, 131–134.

Slobodkin, L. B. (1961). *Growth and Regulation of Animal Populations*, New York: Holt, Rinehart and Winston.

Tong, H. (1990). *Non-linear Time Series: a Dynamical Approach*, Oxford, England: Oxford University Press.

Received 23 February 1999 and accepted 28 June 1999